J|A|C|S
ARTICLES
Published on Web 11/09/2002

Quantum Chemical Calculations on Structural Models of the Catalytic Site of Chymotrypsin: Comparison of Calculated Results with Experimental Data from NMR Spectroscopy

William M. Westler,*,† Frank Weinhold,‡ and John L. Markley†

Contribution from the National Magnetic Resonance Facility at Madison, Department of Biochemistry, and Theoretical Chemistry Institute, Department of Chemistry, University of Wisconsin-Madison, Madison Wisconsin 53706

Received July 17, 2002

Abstract: Hybrid density functional quantum mechanical calculations were used to study the strength of the hydrogen bond between His^{57} $N^{\delta 1}$ and Asp^{102} $O^{\delta 1}$ in chymotrypsin and how it changes along the reaction coordinate. Comparison of experimental shifts with the results of chemical shift calculations on a variety of small molecules, including species containing very strong hydrogen bonds, has validated the overall approach and provided the means for calibrating and correcting the calculated values. Models of the active site of chymotrypsin in its resting state and tetrahedral intermediate state were derived from high-resolution X-ray structures. The distance between His^{57} $N^{\delta 1}$ and Asp^{102} $O^{\delta 1}$ in each model was varied between 2.77 Å (weak hydrogen bond) and 2.50 Å (extremely strong hydrogen bond), and the one-dimensional potential energy surface of the hydrogen-bonded proton (or deuteron/triton) was determined. The zero-point energy, probability distribution, and chemical shift were determined for each distance. Calculated values for NMR chemical shifts, NMR chemical shift differences between ^1H and ^3H, and $^2H/^1H$ fractionation factors were compared with published experimental values. Energies provided by the calculations indicated that the hydrogen bond between His^{57} $N^{\delta 1}$ and Asp^{102} $O^{\delta 1}$ in the chymotrypsin active site increases in strength by 11 kcal mol^{-1} in going from the resting state of the enzyme to the tetrahedral intermediate state. This result confirms the hypothesis that the strengthened hydrogen bond plays an important role in lowering the energy of the transition state and, hence, in the catalytic efficiency of the enzyme. Models of the transition state that best fit the experimental data are consistent with a "strong" hydrogen bond between His^{57} $N^{\delta 1}$ and Asp^{102} $O^{\delta 1}$ but apparently not a "low-barrier" or "very strong" hydrogen bond.

Introduction

The serine proteinases are one of the most studied families of enzymes. While the general mechanism of peptide hydrolysis has been understood for decades, the details of the chemistry that takes place during catalysis are still the subjects of controversy and continuing investigation.[1−4] One focus of interest has been the role of the hydrogen bond between $N^{\delta 1}$ of His^{57} and $O^{\delta 1}$ of Asp^{102} (the chymotrypsinogen numbering system is used throughout this paper). Results from NMR spectroscopy have helped fuel heated debates. Robillard and Shulman[5−7] observed a proton NMR signal in the 15−18 ppm chemical shift range, depending on the solution pH value, and assigned it to the $H^{\delta 1}$ of His^{57}. The chemical shift of this resonance, which lies still farther downfield in transition-state complexes (18.6 to 18.9 ppm), has been interpreted as indicating that a low-barrier hydrogen bond (LBHB) is formed between His^{57} $N^{\delta 1}$ and Asp^{102} $O^{\delta 1}$.[8,9] LBHB formation has been suggested to be the energetic mechanism for the stabilization of the tetrahedral intermediate formed between the active site Ser^{195} O^{γ} and the carbonyl of the scissile peptide bond of the substrate.[10] Additional evidence pointing to an unusually strong hydrogen bond has come from measurements of $^2H/^1H$ fractionation factors in complexes between serine proteinases and transition-state analogue inhibitors.[11−13] The zero-point vibrational energy level for an LBHB is higher than the energy of the transition state for transferring the hydrogen-bonded proton from one Lewis base to the other Lewis base. LBHBs have been

* To whom correspondence should be addressed. Address: 433 Babcock Dr., National Magnetic Resonance Facility at Madison, Department of Biochemistry, University of Wisconsin-Madison, Madison, WI 53706. Phone: 608 263 9599. Fax: 608 262 3759. E-mail: milo@nmrfam.wisc.edu.
† National Magnetic Resonance Facility at Madison, Department of Biochemistry.
‡ Theoretical Chemistry Institute, Department of Chemistry.

(1) Frey, P. A.; Whitt, S. A.; Tobin, J. B. *Science* **1994**, *264*, 1927−1930.
(2) Frey, P. A. *Science* **1995**, *269*, 104−106.
(3) Warshel, A.; Papazyan, A.; Kollman, P. A. *Science* **1995**, *269*, 102−104.
(4) Warshel, A.; Naray-Szabo, G.; Sussman, F.; Hwang, J. K. *Biochemistry* **1989**, *28*, 3629−3637.
(5) Robillard, G.; Shulman, R. G. *J. Mol. Biol.* **1972**, *71*, 507−511.
(6) Robillard, G.; Shulman, R. G. *Ann. N.Y. Acad. Sci.* **1973**, *222*, 220−225.
(7) Robillard, G.; Shulman, R. G. *J. Mol. Biol.* **1974**, *86*, 519−540.
(8) Tobin, J. B.; Whitt, S. A.; Cassidy, C. S.; Frey, P. A. *Biochemistry* **1995**, *34*, 6919−6924.
(9) Golubev, N. S.; Gindin, V. A.; Ligai, S. S.; Smirnov, S. N. *Biochemistry (Moscow)* **1994**, *59*, 447−455.
(10) Cassidy, C. S.; Lin, J.; Frey, P. A. *Biochemistry* **1997**, *36*, 4576−4584.
(11) Markley, J. L.; Westler, W. M. *Biochemistry* **1996**, *35*, 11092−11097.
(12) Halkides, C. J.; Wu, Y. Q.; Murray, C. J. *Biochemistry* **1996**, *35*, 15941−15948.
(13) Hibbert, F.; Emsley, J. *Hydrogen Bonding and Chemical Reactivity*; Academic Press: New York, 1990; pp 255−379.

observed in small compounds such as hydrogen maleate. Whether LBHBs exist in biomolecules, however, is a matter of dispute.[4,14]

The present study was motivated by two factors: (1) advances in computational chemical approaches to modeling complex regions of proteins, and (2) experimental data available for the catalytic center of chymotrypsin and other serine proteinases, in various states along the reaction coordinate, from NMR spectroscopy. Such data include NMR chemical shifts,[5−7,15−19] $^1H/^2H$ fractionation factors,[11,12,20] and NMR chemical shift differences between ^1H and ^3H for the hydrogen bonded between His^{57} $N^{\delta 1}$ and Asp^{102} $O^{\delta 1}$.[21] The computational chemical methods used here were first tested on models of small molecules; the results served to validate the overall approach and provided a means for correcting apparent systematic errors. Then, the methods were applied to models of the "resting" and "tetrahedral, transition-state-like" states of the chymotrypsin active site; these results led to new insights into the catalytic mechanism of this class of enzyme.

Materials and Methods

Computational Methods. The Gaussian 98 computational software package[22] was used for all density functional and chemical shift calculations. Various hybrid density functionals (B3LYP, B1LYP, mPW1PW, mPWPW) and several basis sets (6-31+g*, 6-311+g*) were evaluated in optimizing the potential energy calculations. The GIAO method of chemical shift calculation in Gaussian 98 was used at the B3LYP/6-311++g(2d,2p) level of theory. Calculations of diabatic reaction pathways, eigenvalues, and eigenfunctions were performed in Matlab 5.2.[23] A modified version of the SUPERPOSE routine from Tinker[24] was implemented in Matlab for mass-weighted superposition of molecules.

Chemical Shift Calibration. Tetramethylsilane, methane, ethane, ethyne, ethane, benzene, acetaldehyde, acetic acid dimer, and bifluoride anion were the molecules used to calibrate the regression line comparing calculated and experimental chemical shifts.[25] Model structures for these molecules were obtained by geometry optimization at the B3LYP/6-311g* level of theory. Frequencies were calculated for the ground-state geometries to ensure that no imaginary frequencies were present. The ground-state geometries of these molecules were used in calculating their NMR chemical shifts. Experimental chemical shifts were from Baldridge and Siegel[25] and the Isotec Chemical Shift Reference chart <http://www.isotec.com>.

Chemical shifts for hydrogen maleate, hydrogen dimethylmalonate, and hydrogen phthalate were calculated for both their ground states and the transition states for proton transfer. The B1LYP or mPW1PW method with a basis set of 6-311+g* was used in determining the geometries. Frequencies were calculated to ensure that the correct number of imaginary frequencies were present. Chemical shift values for these compounds were not included in the regression analysis. In addition, a diabatic linear reaction pathway method[26] was used to calculate one-dimensional proton transfer potentials for hydrogen maleate, hydrogen dimethylmalonate, and hydrogen phthalate. A linearly interpolated path of geometries was constructed between the geometries of the ground and transition states. Several more geometries were constructed by linear extrapolation of the geometries beyond the ground state. Invariance of linear and angular momentum along the linear path of geometries was ensured by the mass-weighted superposition of the ground state and the transition state by means of a quaternion method adapted from a routine in Tinker.[24] The chemical shifts and self-consistent field (SCF) energies of the geometries on the linear path were calculated, and a one-dimensional potential energy curve was constructed from a cubic spline fit of the energies. The chemical shift distribution curve was obtained by a cubic spline fit through the calculated chemical shifts for geometries along the diabatic reaction path.

Eigenfunctions and eigenvalues for the potentials were obtained by a discrete variable representation (DVR) method.[27] Diabatic linear reaction pathways for ^2H and ^3H were constructed separately, by replacing the mass of the hydrogen-bonded proton with that of deuterium or tritium. The $^1H/^{2,3}H$ isotope shift is defined as the chemical shift of the ^1H isotope minus that of the $^{2,3}H$ isotope. The vibrationally averaged chemical shift was calculated as the integral of the product of the probability distribution (squared eigenfunction) with the chemical shift distribution across the potential.[28] Vibrationally averaged chemical shifts for energy levels within 3 kT of the zero-point energy level (at 300 K) were obtained and weighted by a Boltzmann distribution.[29]

Comparison of Models of the Active Site with Coordinates from X-ray Structures. Several simplified models for various states of the active site of chymotrypsin were derived (Models I, II, III, and IIIa-d described below). Their geometries were compared with those of the corresponding regions of X-ray structures by calculating root-mean-square deviations (RMSDs) for the differences between the positions of particular heavy atoms in the structures: the carbonyl moiety of Asp^{102}, the imidazole ring, the C^{β}, C^{α}, and N atoms of His^{57}, and the O^{γ} atoms of Ser^{195} and Ser^{214}. The SUPERPOSE function of Tinker[24] was used to obtain the RMSD values.

Model I: Active Site of Chymotrypsin in the First Transition State. The initial atom positions for model I were taken from the coordinates of the X-ray structure of chymotrypsin inhibited by the transition-state analogue inhibitor, phenylalanyl trifluromethyl ketone (N−AcF−CF_3).[30] The model (PDB 6GCH) was simplified in the following way: formyl histamine represents His^{57}; the backbone H^N of His^{57} is hydrogen-bonded to $O^{\delta 2}$ of Asp^{102}, and the imidazole side chain makes two hydrogen bonds (His^{57} $H^{\delta 1}$ to Asp^{102} $O^{\delta 1}$ and His^{57} $H^{\epsilon 2}$ to Ser^{195} O^{γ}). A formaldehyde residue represents the carbonyl of Ser^{214}, which is in close proximity and is probably hydrogen-bonded to $H^{\epsilon 1}$ of His^{57}. Formate represents Asp^{102}; and a water molecule

(14) Ash, E. L.; Sudmeier, J. L.; Defabo, E. C.; Bachovchin, W. W. *Science* **1997**, *278*, 1128−1132.
(15) Markley, J. L.; Porubcan, M. A. *J. Mol. Biol.* **1976**, *102*, 487−509.
(16) Markley, J. L.; Ibañez, I. B. *Biochemistry* **1978**, *17*, 4627−4640.
(17) Porubcan, M. A.; Neves, D. E.; Rausch, S. K.; Markley, J. L. *Biochemistry* **1978**, *17*, 4640−4647.
(18) Porubcan, M. A.; Westler, W. M.; Ibañez, I. B.; Markley, J. L. *Biochemistry* **1979**, *18*, 4108−4116.
(19) Kaslik, G.; Westler, W. M.; Gráf, L.; Markley, J. L. *Arch. Biochem. Biophys.* **1999**, *362*, 254−264.
(20) Lin, J.; Westler, W. M.; Cleland, W. W.; Markley, J. L.; Frey, P. A. *Proc. Natl. Acad. Sci. U.S.A.* **1998**, *95*, 14664−14668.
(21) Westler, W. M.; Frey, P. A.; Lin, J.; Wemmer, D. E.; Morimoto, H.; Williams, P. G.; Markley, J. L. *J. Am. Chem. Soc.* **2002**, *124*, 4196−4197.
(22) Frisch, M. J.; Trucks, G. W.; Schlegel, G. E.; Scuseria, G. E.; Robb, M. A.; Cheeseman, J. R.; Zakrzewski, V. G.; Montgomery, J. A., Jr.; Stratmann, R. E.; Burant, J. C.; Dapprich, S.; Millam, J. M.; Daniels, A. D.; Kudin, K. N.; Strain, M. C.; Farkas, O.; Tomasi, J.; Barone, V.; Cossi, M.; Cammi, R.; Mennucci, B.; Pomelli, C.; Adamo, C.; Clifford, S.; Ochtershki, J.; Petersson, G. A.; Ayala, P. Y.; Cui, Q.; Morokuma, K.; Malick, D. K.; Rabuck, A. D.; Raghavachari, K.; Foresman, J. B.; Cioslowski, J.; Ortiz, J. V.; Baboul, A. G.; Stefanov, B. B.; Liu, G.; Liashenko, A.; Piskorz, P.; Komaromi, I.; Gomperts, R.; Martin, R. L.; Fox, D. J.; Keith, T.; Al-Laham, M. A.; Peng, C. Y.; Nanayakkara, A.; Challacombe, M.; Gill, P. M. W.; Johnson, B.; Chen, W.; Wong, M. W.; Andres, J. L.; Gonzalez, C.; Head-Gordon, M.; Replogle, E. S.; Pople, J. A. *Gaussian 98*, revision A.9; Gaussian Inc.: Pittsburgh, PA, 1998.
(23) *MATLAB*, 5.2; The Mathworks, Inc.: Natic, MA, 2001.
(24) Ponder, J. W. *TINKER: Software Tools for Molecular Design*, version 3.6; Washington University School of Medicine: St. Louis, MO, 1998.
(25) Baldridge, K. K.; Siegel, J. S. *J. Phys. Chem. A* **1999**, *103*, 4038−4042.
(26) Miller, W. H.; Ruf, B. A.; Chang, Y. T. *J. Chem. Phys.* **1988**, *89*, 6298−6304.
(27) Colbert, D. T.; Miller, W. H. *J. Chem. Phys.* **1992**, *96*, 1982−1991.
(28) Garcia-Viloca, M.; Gelabert, R.; González-Lafont, A.; Moreno, M.; Lluch, J. M. *J. Phys. Chem. A* **1997**, *101*, 8727−8733.
(29) Garcia-Viloca, M.; Gelabart, R.; Gonzalez_Lafont, A.; Moreno, M.; Lluch, J. M. *J. Am. Chem. Soc.* **1998**, *120*, 10203−10209.
(30) Brady, K.; Wei, A.-Z.; Ringe, D.; Abeles, R. H. *Biochemistry* **1990**, *29*, 7600−7607.

represents the crystallographic water molecule hydrogen bonded to Ser^{214}. 1,1,1-trifluoroacetone represents the transition-state analogue inhibitor. N-formyl-glycyl-N-glycyl-N-2-hydroxyethylamine represents the "oxyanion hole" (residues 193−195 of the enzyme) and the side chain hydroxyl of Ser^{195}. Three additional water molecules were added to satisfy the hydrogen-bonding valances of the carbonyl moieties of residues 192−195. This model is an extension of one developed by Weinhold for the resting enzyme (Model II described below) and is similar to that of Shokhen and Albeck.[31] This large complex was subjected to unconstrained geometry optimization at the mPWPW/6-31+g* level of theory and was stable.

The optimization was performed starting from a tetrahedral species with the Ser^{195} hydroxyl bound to the carbonyl of the 1,1,1-trifluoroacetone. Upon optimization of this tetrahedral complex, the Ser^{195} hydroxyl proton was transferred to the imidazole $N^{\epsilon 2}$ of His^{57}.

Model II: Resting State Active Site. The model used to represent the active site of chymotrypsin in its negatively charged, resting state was that described by Weinhold.[32] As in Model I, formyl histamine represents His^{57}, formate represents Asp^{102}, and three water molecules represent Ser^{195}, Ser^{214}, and a crystallographic water molecule hydrogen bonded to Ser^{214}. In this model, a formal negative charge resides on the formate group, which represents Asp^{102}. Unconstrained geometry optimization was at the mPW1PW/6-311+g* level of theory. This model was stable to unconstrained geometry optimization. A frequency calculation gave no imaginary frequencies.

Model III: Active Site of Free Chymotrypsin with a Protonated Imidazole. Model II (the model for the resting enzyme) has a formal negative charge on Asp^{102} and a neutral charge on the imidazole of His^{57}. This initial model was converted into one that mimics the catalytic triad with a protonated imidazole by adding a proton to $N^{\epsilon 2}$ of His^{57} and optimizing the geometry of the protons while holding all heavy atoms fixed. During unconstrained geometry optimization, this structure moved away from the experimental geometry. All further optimizations using this model were calculated with the heavy atom positions fixed.

Potential Energy Curves for Proton Transfer. Four models (Models IIIa, IIIb, IIIc, and IIId) were derived from Model III to generate the one-dimensional proton-transfer potential energy curves of His $H^{\delta 1}$ as a function of the His^{57} $N^{\delta 1}$−Asp^{102} $O^{\delta 1}$ distance. Starting from Model III, the distance between the $N^{\delta 1}$ of His^{57} and the $O^{\delta 1}$ of Asp^{102} was constrained to a series of fixed values: IIIa, 2.77 Å; IIIb, 2.70 Å; IIIc, 2.60 Å; IIId, 2.50 Å.

Each of these models, in turn, was used to generate a series of submodels in which the heavy atoms were fixed, and only the position of the proton between $N^{\delta 1}$ of His^{57} and $O^{\delta 1}$ of Asp^{102} was varied. The resulting geometries of the submodels were optimized with heavy atoms and protons bound to carbon fixed but with all other degrees of freedom for oxygen- or nitrogen-bound protons unconstrained. The resulting data were fitted with a cubic spline to generate the one-dimensional potential energy curve. The eigenvalues and eigenfunctions were determined for these potentials. To simulate isotope effects on zero-point energies and chemical shifts, the mass of the particle in the potential was adjusted from that of ^1H to that of ^3H.

Computation of Fractionation Factors. The $^1H/^2H$ fractionation factor is defined as the equilibrium between protonated protein and deuterated protein in an isotopically mixed solvent (Scheme 1).[33] In Scheme 1, L represents either ^1H or ^2H. The symbol $^2H(L_2O)$ indicates

Scheme 1

$$XH + D(L_2O) \rightleftharpoons XD + H(L_2O)$$

$$\phi_{XL} = [(XD)/(XH)]\,(H/D)_{L_2O}$$

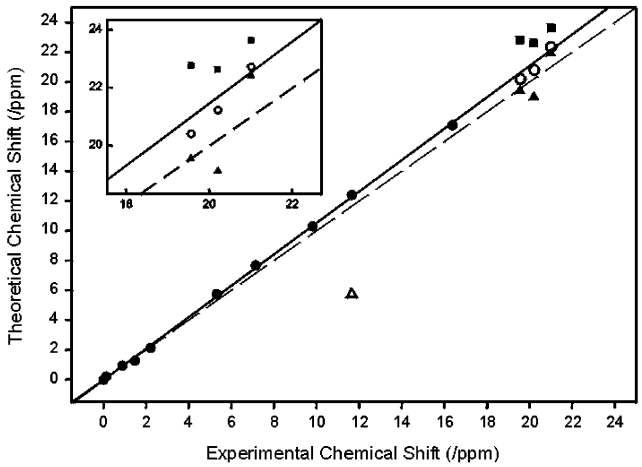

Figure 1. Correlation between calculated and experimental proton chemical shifts for model compounds used in developing a correction factor for calculated chemical shifts. The points, in order of increasing chemical shifts tetra-methylsilane (defined as the zero chemical shift), methane, ethane, ethyne, ethane, benzene, acetaldehyde, acetic acid dimer, and bifluoride anion. Experimental chemical shifts were from Baldridge[25] and the Isotec chemical shift reference chart. These data, indicated on the figure by filled circles, were used to calculate the chemical shift regression line (solid line). The dashed line is of unit slope. Chemical shift calculations were carried out for additional species, not used in the calibration series; their correlations with experimental chemical shifts are shown in the figure as indicated by other symbols (see below). As discussed in the text, the point for the acetic acid monomer (open triangle) lies off the line; it was not used in the regression analysis, but the calculated value for the acetic acid dimer, the predominant species in the liquid, was used. Models representing the (filled triangles) ground state, (filled squares) transition state for proton transfer, and (open circles) vibrationally averaged state were evaluated for hydrogen phthalate (δ_{exptl} = 21.0 ppm), hydrogen maleate (δ_{exptl} = 20.2 ppm), and hydrogen 2,2-dimethylmalonate(δ_{exptl} = 19.6 ppm). The region of the plot including these data is enlarged in the inset. In each case, it is clear that the vibrationally averaged model provided the best fit to the calibration curve.

that the ^2H atom is involved in the equilibrium and the atom comes from solvent

$$\phi_n = e^{\frac{hc}{kT}(\mathrm{ZPE}_{1H,n} - \mathrm{ZPE}_{2H,n} - \mathrm{ZPE}_{1H,L_2O} + \mathrm{ZPE}_{2H,L_2O})} \quad (1)$$

containing both isotopes. The fractionation factor ϕ_{XL} is the equilibrium constant for this reaction. Fractionation factors were estimated from the one-dimensional zero-point energy (ZPE) levels for the molecule of interest and those of the solvent (eq 1).[33] The ZPE levels are expressed in cm^{-1}. The subscript *n* refers to the site on the molecule under study. A cyclic pentamer of water molecules was used as the water model.[34]

Results

Validation and Calibration of Calculated Chemical Shifts. Methods used to calculate chemical shifts for the chymotrypsin active site were validated and calibrated by reference to results from calculations on a series of small molecules, which were compared with experimental values. The GIAO method at the B3LYP/6-311++g(2d,2p) level of theory was used to calculate the chemical shielding values that were converted to chemical shifts by reference to the calculated chemical shielding value for tetramethylsilane (TMS), whose chemical shift was set to zero. A linear correlation fit of the theoretical versus experimental chemical shifts yielded a line with a slope of 1.055 and an intercept of −0.024 ppm (Figure 1). Although the correction is small for chemical shifts less than 10 ppm from TMS, the

(31) Shokhen, M.; Albeck, A. *Proteins: Struct., Funct., Genet.* **2000**, *40*, 154−167.
(32) Weinhold, F. *J. Mol. Struct. (THEOCHEM)* **1997**, *398*−*399*, 181−197.
(33) Kreevoy, M. M.; Liang, T.-M. *J. Am. Chem. Soc.* **1980**, *102*, 3315−3322.
(34) Weinhold, F. *J. Chem. Phys.* **1998**, *109*, 373−384.

Table 1. Chemical Shifts and Isotope Shifts Calculated for Three Organic Acid Salts that Contain Strong, Short Hydrogen Bonds and Comparison with Experiment ("n/a" Indicates Experimental Data Not Available)

species investigated	model[a] used for calculations	^{1}H chemical shift (/ppm)		^{1}H–^{2}H chemical shift difference (/ppm)		^{1}H–^{3}H chemical shift difference (/ppm)	
		theory	expt	theory	expt	theory	expt
FHF^-	TS	16.2	16.4[b]	n/a	n/a	n/a	n/a
hydrogen maleate	VA	20.2	20.2[c]	−0.11	−0.03[c]	0.00	−0.07[c]
	GS	17.9		n/a		n/a	
	TS	21.3		n/a		n/a	
hydrogen 2,2-dimethylmalonate	VA	19.2	19.6[d]	0.00	n/a	0.01	n/a
	GS	18.4				n/a	
	TS	21.4				n/a	
hydrogen phthalate	VA	21.4	21.0[c]	−0.03	−0.15[c]	0.05	−0.25[c]
	GS	21.3		n/a		n/a	
	TS	22.3		n/a		n/a	

[a] Abbreviations: VA: vibrationally averaged; GS, ground state; TS, transition state. [b] Values from ref 13. [c] Values from ref 40. [d] Values from ref 1.

correction is about 1 ppm for larger chemical shifts, such as those associated with putative LBHBs (~20 ppm). The slope bias correction was incorporated into all calculated chemical shifts reported below.

The slope bias may arise from the poor behavior of single determinant wave functions near dissociation. Similar effects have been seen in calculation of vibrational frequencies, which require scaling of the calculated frequencies to match experimental values.[35] The known correlation between experimental chemical shifts and vibrational frequencies suggests that the biases seen in frequency and chemical shift calculations may be related.[36]

For acetic acid, the predominant species present in solution is the dimer.[37] In agreement with this, the chemical shift calculated for monomeric acetic acid (5.45 ppm) falls far from the experimental value (11.65 ppm), whereas the chemical shift calculated for dimeric acetic acid (11.8 ppm) agrees closely with experiment.

Calculation of Chemical Shifts and Isotope Shifts for Molecules with Short, Strong Hydrogen Bonds. The bifluoride anion FHF^-, hydrogen maleate, hydrogen 2,2-dimethylmalonate, and hydrogen phthalate are model compounds that exhibit extremely short, strong (in certain cases, low-barrier) hydrogen bonds.[13,38] FHF^- has an experimental and calculated ground-state geometry that is symmetric, with the hydrogen atom equidistant from the two fluorine atoms.[39] The calculated chemical shift for the symmetric species (16.2 ppm) is close to the experimental shift (16.4 ppm). [13] As shown in Figure 1 (enlarged in the inset), the calculated chemical shifts for the ground-state geometries of hydrogen maleate (17.9 ppm) and hydrogen 2,2-dimethylmalonate (18.4 ppm) differ significantly from the respective experimental values, 20.2 and 19.6 ppm.[1] The chemical shift calculated for hydrogen phthalate in the ground-state configuration (21.3 ppm) is close to the experimental value (21.0 ppm).[40] Since these molecules may exhibit LBHBs, it might be expected that the true molecular geometry more closely resembles the transition state for proton transfer between the two carboxylate oxygen atoms. The calculated chemical shifts for the proton-transfer transition states in these molecules, however, does not reproduce the experimental values (Figure 1 and Table 1).

To calculate accurate chemical shifts for these molecules, it was necessary to construct a more accurate model, one that includes the effects of vibrational averaging. The "diabatic reaction pathway" method of Miller[26] was used to construct one-dimensional potentials for proton transfer. In this approach, a linearly interpolated (and extrapolated) set of structures is constructed using the geometries of the ground state and the transition state of interest. The requirement that no translational or rotational motion is generated along the path between the ground and transition states was met by performing a mass-weighted superposition of the ground- and transition-state geometries. Intermediate geometries were constructed by linear interpolation of the spatial coordinates between the superposed end points. To complete the potential, structures were linearly extrapolated beyond the ground-state end point. Individual sets of structures were generated for each isotopic composition (i.e., ^{1}H, ^{2}H, or ^{3}H in the hydrogen bond). The diabatic pathway represents the shortest path between two states, with all other vibrational degrees of freedom being orthogonal.[26] This method is especially useful in the description of proton-transfer reactions, in which the proton "cuts the corners" in the potential energy surface instead of following the adiabatic, minimum energy pathway.[26]

Figure 2A shows the potential calculated by this method for hydrogen maleate with eigenvalues within 3 kT of the zero-point energy at 300 K, the probability distributions (squares of the eigenfunctions) at each of these energy levels, and the chemical shift distributions across the potential well. At this level of theory, the zero-point energy level lies slightly above the transition-state barrier between the two wells. This is a classic example of a low-barrier hydrogen bond. The diffuse probability distribution at the zero-point energy indicates that the proton is "smeared" between the two oxygen atoms of the carboxylate moieties. The nodal features of the higher energy probability distributions tend to localize the proton toward the oxygen atoms. At a given temperature, the three energy levels shown will be populated to an extent dictated by the Boltzmann distribution. The chemical shift distribution was calculated from the chemical shifts of individual structures along the diabatic reaction path. The vibrationally averaged chemical shift was obtained as a Boltzmann-weighted average of the probability-weighted chemical shift across the populated levels. The vibrationally averaged chemical shift for hydrogen maleate

(35) Foresman, J. B.; Frisch, A. E.. *Exploring Chemistry with Electronic Structure Methods*; Gaussian, Inc.: Pittsburgh, PA, 1996.
(36) Brunner, E.; Karge, H. G.; Pfeifer, H. *Z. Phys. Chem. (Munich)* **1992**, *176*, 173−183.
(37) Goldman, M. A.; Emerson, M. T. *J. Phys. Chem.* **1973**, *77*, 2295−2299.
(38) Allen, K. N.; Bellamacina, C. R.; Ding, X. C.; Jeffery, C. J.; Mattos, C.; Petsko, G. A.; Ringe, D. *J. Phys. Chem.* **1996**, *100*, 2605−2611.
(39) Bozorth, R. M. The Crystal Structure of Potassium Hydrogen Flouride. *J. Am. Chem. Soc.* **1923**, *45*, 2128−2132.
(40) Altman, L. J.; Laungani, P.; Gunnarsson, G.; Wennerstrom, H.; Forsen, S. *J. Am. Chem. Soc.* **1978**, *100*, 8264−8265.

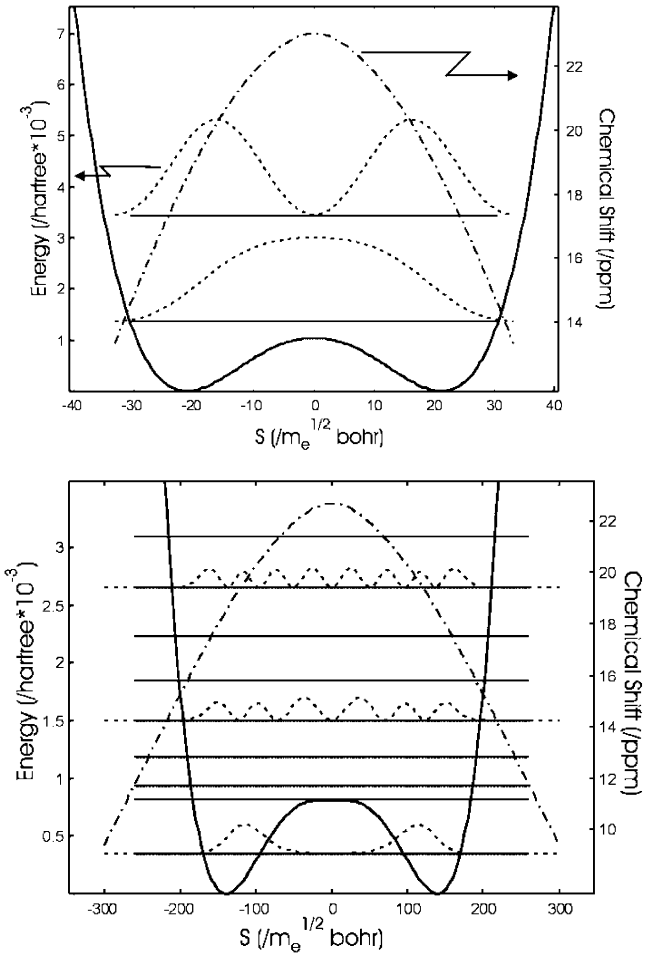

Figure 2. Potential energy levels for eigenvalues within 3 kT (at 300 K) of the zero-point energy calculated by the diabatic reaction pathway method (−),[26] probability distributions (squares of the eigenfunctions) (− −), and chemical shift distributions across the potential well calculated by the GIAO method at the B3LYP/6-311++g(2d,2p) level of theory (−•−): (A) hydrogen maleate; (B) hydrogen 2,2-dimethylmalonate. The calculated results are shown in Table 1.

(Table 1) is different both from that of the ground state and that of the transition state, because the probability distribution averages chemical shifts that vary across the potential from about 14 ppm to 23 ppm.

Figure 2B shows calculated potential energy levels, probability distributions, and chemical shift distributions for hydrogen 2,2-dimethylmalonate. In this molecule, the experimental chemical shift at room temperature is 19.6 ppm, which could be interpreted as indicating that this molecule contains a low-barrier hydrogen bond.[1] The calculated vibrationally averaged, room-temperature chemical shift was 19.2 ppm, in agreement with experiment. However, at the level of theory used here, the zero-point energy is well below the energy of the transition state. The large calculated vibrationally averaged chemical shift is the result of occupancy of energy levels within 3*kT of the zero-point energy level and concomitant spreading of the proton probability distribution. Thus, the chemical shift should be temperature dependent. This was borne out by the calculation of a chemical shift of 18.8 ppm at 0 K. This large temperature dependence should be observable experimentally; indeed, temperature dependencies on this order have been observed for other hydrogen-bonded species.[29] These calculations suggest that measurement of a room-temperature proton chemical shift >19 ppm is insufficient to indicate the presence of an LBHB.

Barich et al. have concluded that electron correlation is important in the accurate calculation of chemical shifts in strong hydrogen bonds.[41] Ground- and transition-state values obtained from their MP2 calculations for maleate are 21.5 and 20.4 ppm and for dimethylmalonate, the ground- and transition-state values are 21.3 and 22.5 ppm. Comparison with the values in Table 1 shows that the MP2 results give larger shifts than the hybrid density functional used here. However, the Boltzmann averaged results from the MP2 calculations, 22.3 ppm for maleate and 22.2 ppm for dimethylmalonate, are significantly farther away, ~2 ppm, from the experimental results than the vibrationally averaged results given here. While correlation appears important in chemical shift calculations when compared to Hartree−Fock calculations, the electron correlation that is implicit in density functional theory, DFT, along with the vibrational averaging of the chemical shifts appears to support accurate shift results. One significant difference between these two studies is that the MP2 calculations predict that dimethylmalonate has a single-well potential while the results given here indicate that the potential is double-welled with a high barrier. The temperature dependence predicted here for dimethylmalonate suggests an experimental resolution to this discrepancy.

The inset in Figure 1 (correlation between experimental and uncorrected calculated chemical shifts) shows an expansion of the region with chemical shifts of the hydrogen-bonded protons in hydrogen maleate, hydrogen 2,2-dimethylmalonate, and hydrogen phthalate. The filled triangles and squares represent the ground and transition states, respectively, and the open circles represent the vibrationally averaged state, with chemical shifts obtained from the calculated probability distributions. The agreement of the vibrationally averaged chemical shifts with the experimental data is quite good (when the systematic bias in the chemical shifts is taken into account).

For an element confined to a potential well, isotopes with heavier masses have lower zero-point energies; consequently, the positional probability distribution is different for different masses. Since the chemical shift variation across a potential is independent of the probability distribution, vibrationally averaged chemical shifts are expected to be different for different isotopes, even in a harmonic potential. Proton-deuterium and proton-triton isotope shifts were calculated for hydrogen maleate, hydrogen 2,2-dimethylmalonate, and hydrogen phthalate (Table 1). All of the isotope shifts are close to zero and are reasonably consistent with available experimental data. Some changes in the potential, and thus in the isotope shifts, are expected as the result of small changes in the heavy atom distances upon substitution of the various hydrogen isotopes (Ubbelohde effect).[42,43] These effects were not modeled in this investigation.

Computation of Chemical Shifts and $^3H-^1H$ Isotope Shifts in Serine Proteinase Active Site Models. Unconstrained geometry optimization of Model I gave a structure (Figure 3) with an RMSD of 0.61 Å to the X-ray structure of trifluoromethyl ketone inhibited chymotrypsin (6GCH).[30] The robustness of this geometry in the absence of the rest of the protein is remarkable. This structure is internally stable, suggesting that

(41) Barich, D. H.; Nicholas, J. B.; Haw, J. F. *J. Phys. Chem. A* **2001**, *105*, 4708−4715.
(42) Robertson, J. M.; Ubbelohde, A. R. *Proc. R. Soc.* **1939**, *A170*, 222−240.
(43) Ubbelohde, A. R.; Woodward, I. *Proc. R. Soc.* **1945**, *A185*, 448−464.

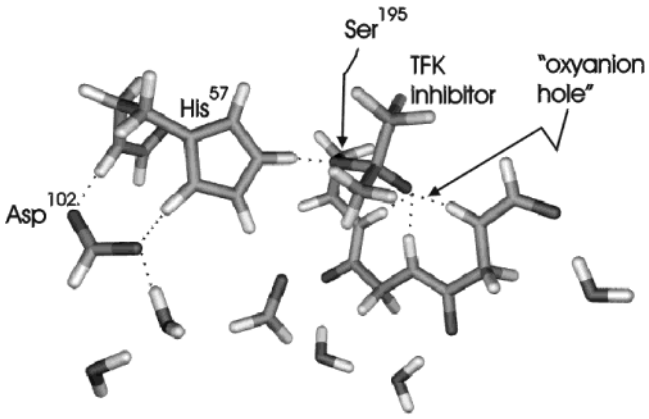

Figure 3. The active site of chymotrypsin in its first transition state: Model I. The initial atom positions were taken from the coordinates of the X-ray structure of phenylalanyl-trifluromethyl ketone-inhibited chymotrypsin.[30] The model was simplified in the following way. 1,1,1-trifluoroacetone was used to represent the transition-state analogue inhibitor. N-formyl-glycyl-N-glycyl-N-2-hydroxyethylamine was used to represent of the "oxyanion hole" and the side chain hydroxyl of Ser^{195}. A formaldehyde residue was used to represent the carbonyl of Ser^{214}, which is in close proximity and is probably hydrogen-bonded to $H^{\epsilon 1}$ of His^{57}. Three additional water molecules were added to satisfy the hydrogen-bonding valances of the carbonyl moieties of residues 192−195. The model shown here is the result of unconstrained geometry optimization at the mPWPW/6-31+g* level of theory.

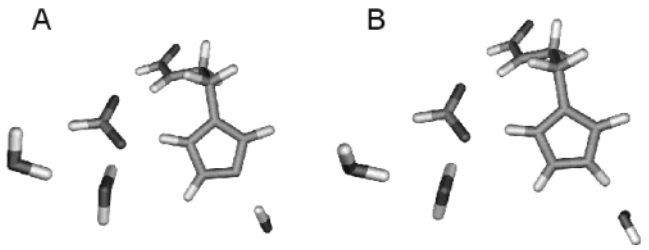

Figure 4. Models of the resting state of chymotrypsin. (A) Model II: resting state at high pH with His^{57} deprotonated. In this model, formyl histamine represents His^{57}, formate represents Asp^{102}, and three water molecules represent Ser^{195}, Ser^{214}, and the water molecule hydrogen bonded to Ser^{214}. A formal negative charge resides on the formate group, which represents Asp^{102}. The model shown was geometry optimized at the mpw1pw/6-311+g* level of theory and was stable to unconstrained geometry optimization. (B) Model III: resting state at low pH with His^{57} protonated (as a simplified model for the transition state in catalysis). This model was created from Model II by adding a proton to $N^{\epsilon 2}$ of His^{57} and optimizing the geometry of the protons while holding all heavy atoms fixed. This model could not be improved by unconstrained geometry optimization because the structure moved away from the experimental geometry.

the proposed tetrahedral intermediate in catalysis may have similar stability. The distance between $O^{\delta 1}$ of Asp^{102} and $N^{\delta 1}$ of His^{57} in this model is 2.66 Å. The calculated chemical shift for $H^{\delta 1}$ is 18.3 ppm. This value is slightly less than the values obtained experimentally. If the proton is in a potential well with significant anharmonicity, then it is expected that the chemical shift would move to higher frequencies (higher ppm). While the experimental geometries and chemical shifts are reproduced fairly accurately with Model I, this model is too large to permit detailed computational analyses.

Model II (Figure 4A), which contains fewer atoms than Model I, was chosen to represent the negatively charged active site of the resting enzyme for the calculations. Like Model I, Model II is stable to unconstrained geometry optimization in the gas phase.[32] Again, the fact that the geometry is conserved in the absence of the rest of the protein indicates that this structure is relatively stable. The optimized geometry had an RMSD of 0.37 Å to the X-ray structure of N−AcF−CF_3–chymotrypsin (6GCH).[30] Addition of a proton to the imidazole of Model II yielded Model III (Figure 4B), which represents the structure of the active site at the stage of the putative tetrahedral intermediate. At this point in the catalytic mechanism, the proton of Ser^{195} H^{γ} has been transferred to $N^{\epsilon 2}$ of His^{57} as, simultaneously, a tetrahedral species is formed between the Ser^{195} $O\gamma$ and the scissile carbonyl of the substrate. Upon unconstrained geometry optimization, the cluster of Model III does not retain a geometry similar to the X-ray structure. The structure of the protein matrix surrounding the active site is apparently required to stabilize the active site residues during catalysis. With the introduction of the oxyanion hole as in Model I, a stable structure is generated. At the expense of some accuracy, this smaller model was used to calculate the properties of the active site residues. In all optimizations using Model III, the heavy atom positions were fixed.

The eigenvalues, probability distributions, and chemical shift distributions for the one-dimensional potential energy curves for Model III a−d are shown in Figure 5. Also in Figure 5 are shown the zero-point energy and the next higher vibrational energy level for each potential. A comparison of the theoretical and experimental values of the chemical shifts for the active site of trifluoromethyl ketone-inhibited chymotrypsin are collected in Table 2.

Figure 6A is a plot of the chemical shift of $H^{\delta 1}$ versus the distance between $O^{\delta 1}$ of Asp^{102} and $N^{\delta 1}$ of His^{57} in Model III. The points were fitted to a cubic spline; the resulting line has no theoretical significance. The two horizontal lines demarcate the range of values observed experimentally, and the filled dot is at the intersection of the $O^{\delta 1}-N^{\delta 1}$ distance and the calculated chemical shift from Model I. The sensitivity of the chemical shift to the change in $O^{\delta 1}-N^{\delta 1}$ distance is highly variable (Figure 6A). For N−O distances near 2.66 Å, the slope of the curve is about −20 ppm/Å, whereas for N−O distances near 2.5 Å, the slope is −3.5 ppm/Å. Figure 6B is a plot of the calculated $^1H-^3H$ isotope shift for model IIIa−d. The solid line, which is a cubic spline fit to the data, has no theoretical significance. The distance dependence of the isotope shift is opposite to that of the chemical shift. At N−O distances near 2.66 Å, the slope of the curve is small (0.9 ppm/Å); whereas at an N−O distance near 2.5 Å, the slope is 8.4 ppm/Å.

Computation of $^1H/^2H$ Fractionation Factors in Serine Proteinase Active Site Models. The computed fractionation factors for model IIIa−d are collected in Table 2 along with the experimental values for inhibited chymotrypsin. As the distance between the imidazole nitrogen and the carboxylate oxygen decreases, the magnitude of the fractionation factor also decreases, reaching a minimum at the shortest distance computed. The calculation gives the proper trend, but the calculated values do not agree very well with experiment.

Discussion

Chemical Shifts. Other groups have reported on the reliability of proton chemical shift calculations for small organic molecules.[25,44] Figure 1 shows that the correlation can be extended to molecules with chemical shifts greater than that of benzene,

(44) Rablen, P. R.; Pearlman, S. A.; Finkbiner, J. *J. Phys. Chem. A* **1999**, *103*, 7357−7363.

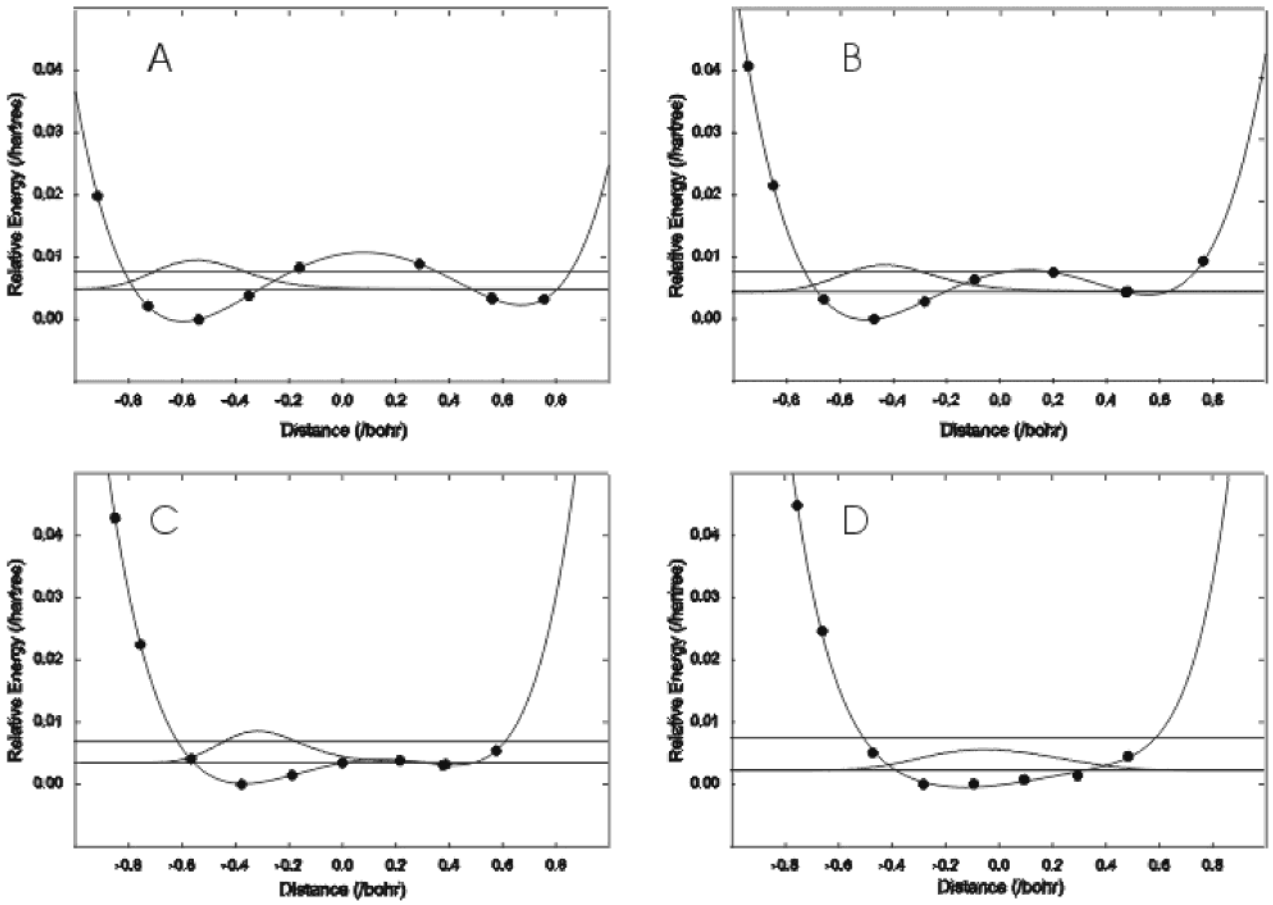

Figure 5. Eigenvalues, probability distributions, and chemical shift distributions for the one-dimensional potential energy curves of Model III a−d (see text). The horizontal lines indicate the zero-point energy and the next higher vibrational energy level for each potential. In Model III a−d, the distance between the $N^{\delta 1}$ of His^{57} and the $O^{\delta 1}$ of Asp^{102} was constrained at the following values: (A) 2.77 Å, (B) 2.70 Å, (C) 2.60 Å, (D) 2.50 Å.

Table 2. Comparison of the Experimental and Calculated Values for the Chemical Shifts, Isotope Shifts, and Fractionation Factors

Experimental

inhibitor	Asp^{102} $O^{\delta 1}$ His^{57} $N^{\delta 1}$ distance (/Å)[a]	$H^{\delta 1}$ (/ppm)[b]	$1H^{\delta 1}$–$3H^{\delta 1}$ (/ppm)[c]	$^1H/^2H$ fractionation factor ϕ[d]
N−AcF−CF_3	2.57	18.61	0.63	0.32
N−AcGF−CF_3		18.66		0.34
N−AcVF−CF_3		18.91	0.65	0.39
N−AcLF−CF_3	2.62	18.95	0.68	0.43

Calculated

model	Asp^{102} $O^{\delta 1}$ His^{57} $N^{\delta 1}$ distance (/Å)	vibrationally averaged ^1H chemical shift (/ppm)	^1H–^3H chemical shift difference (/ppm)	$^1H/^2H$ fractionation factor ϕ
IIIa	2.77	17.02	0.61	1.03
IIIb	2.7	19.03	0.52	0.77
IIIc	2.6	20.91	0.39	0.50
IIId	2.5	21.70	−0.14	0.48

[a] Values from ref 30. [b] Values from ref 50. [c] Values from ref 21. [d] Values from ref 20.

including hydrogen-bonded species. However, for systems with very strong hydrogen bonds, such as hydrogen maleate, hydrogen dimethylmalonate, and hydrogen phthalate, the relationship between experimental chemical shifts and calculated chemical shifts derived from ground-state geometries no longer holds. As an example, the chemical shift calculated for hydrogen maleate on the basis of its ground-state geometry is 2.3 ppm smaller than the experimental value in a nonpolar solvent. The chemical shift calculated on the basis of the transition state for proton transfer is 1.1 ppm larger than the experimental value. This seems somewhat counterintuitive in that hydrogen maleate is thought to contain a strong, short hydrogen bond, perhaps even a low-barrier hydrogen bond, in which the position of the hydrogen-bonded proton lies symmetrically between the oxygen atoms. The calculated transition-state geometry, which is also symmetric, should therefore be a reasonable approximation of the symmetric experimental geometry. However, even after the slope correction of the calculated chemical shift, the experimental chemical shift is not reproduced. The probability distribution, which is the square of the wave function, for the hydrogen maleate potential at the zero-point energy level is dispersed across the potential. The proton does not behave as a point entity, but "samples" regions of the potential that have lower chemical shifts than that of the midpoint. The averaged chemical shift is, therefore, lower than that of the transition state, in which the proton is taken as a point entity and, therefore, samples only the midpoint of the chemical shift distribution curve.

Isotope Shifts. The magnitudes and the trends for the calculated isotope shifts for hydrogen maleate, hydrogen dimethylmalonate, and hydrogen phthalate are fairly consistent with the experimental values (Table 1). The detailed shape of the potential is critical for an accurate determination of the isotope shift. The Ubbleohde effect, in which the distance between

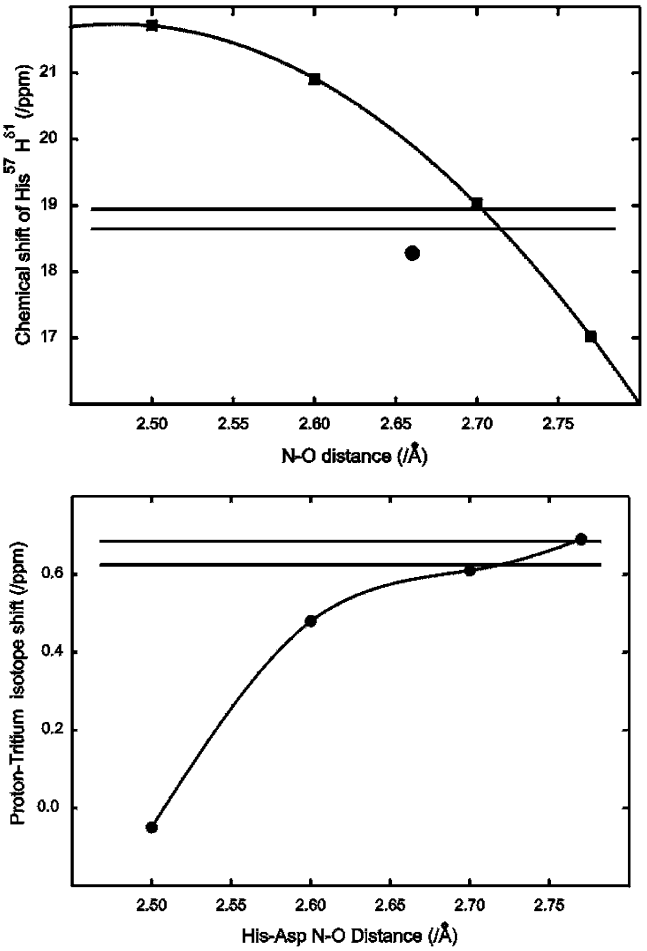

Figure 6. Results from calculations on Model III a−d that have varying distances between $N^{\delta 1}$ of His^{57} and the $O^{\delta 1}$ of Asp^{102}: (A) calculated ^1H chemical shifts as a function of N−O distance; (B) calculated $^1H-^3H$ isotope shifts as a function of N−O distance.

the heavy atoms is changed by substitution with proton isomers, was not taken into consideration in this study, and this simplification contributed to the uncertainty in the calculated potential. Nevertheless, the overall quality agreement between the calculated and experimental chemical shifts and isotope shifts for strongly hydrogen-bonded species is quite good and suggests that the same approach may be applicable to larger macromolecular systems.

Fractionation Factors. The calculated fractionation factors follow the correct trend but do not accurately reproduce the experimental values. The zero-point energies from which the fractionation factors are calculated are sensitive to the detailed shape of the potential well and to other vibrational modes. Furthermore, the calculation involves both the model under study as well as the model of the solvent. These factors likely are responsible for the limitations of the calculations.

Active Site of Chymotrypsin. The distances between the Asp^{102} $O^{\delta 1}$ and the His^{57} $N^{\delta 1}$, determined from X-ray structures of a series of complexes between chymotrypsin and different trifluoromethyl ketone transition-state analogue inhibitors, ranged from 2.77 to 2.50 Å.[45] The resolution of each of the X-ray structures was 1.8 Å. A recent refinement of the N-Acetyl-Leu-Phe chymotrypsin structure solved at 1.3 Å gives the N−O distance as 2.6 Å.[46] As a rule of thumb, the coordinate accuracy for the most highly resolved atoms in an X-ray structure is expected to be about one-tenth the resolution.[47] Thus, the uncertainty in the distance between Asp^{102} $O^{\delta 1}$ and His^{57} $N^{\delta 1}$ is comparable to differences observed for different inhibitors. Even the 1.3 Å structure is expected to have uncertainties of about 0.1 Å. The magnitude of the structural uncertainties preclude useful correlations between atomic distances and properties of the complexes, such as binding constants or chemical shifts. For this reason, we have taken the approach of using the X-ray structures as starting points for geometry optimization of structural models prior to carrying out the computations.

Model I (Figure 3) consists of the Asp-His dyad, the tetrahedral species formed from the hydroxyl oxygen of serine and the carbonyl of the inhibitor, the oxyanion hole, and a few molecules added to satisfy hydrogen-bonding valances. This model is remarkably stable to unconstrained geometry optimization, and the positions of these groups in the resultant structure are very similar to their corresponding positions in the X-ray structure of chymotrypsin. As one would expect from the standard mechanism of the serine proteinases, the imidazole side chain of His^{57} binds the hydroxyl proton of Ser^{195} upon formation of the tetrahedral intermediate. The distance between the Asp^{102} $O^{\delta 1}$ and the His^{57} $N^{\delta 1}$ in Model I (2.65 Å) is about 0.1 Å shorter than the same distance found in Model II (2.78 Å), which represents the active site of the resting enzyme. Also, the newly formed, negatively charged carbonyl oxygen is hydrogen bonded to three peptide NH moieties in the oxyanion hole. This is very similar to the overall topology of the complex as observed in X-ray structures. The N−O distance in Model I is only 0.05 Å longer than that observed in the crystal structure solved at 1.3 Å.[46] Chemical shift calculation on Model I gave a chemical shift for His^{57} $^1H^{\delta 1}$ of 18.3 ppm. This value is close the experimental values obtained for the four different inhibitor complexes (Table 2). Vibrational averaging will cause the proton chemical shift to move downfield making the correspondence between theory and experiment even better.

Figure 7 is a plot of the energies of Model IIIa−d. The energy of Model III is lowered by about 11 kcal as the result of decreasing the N−O distance from the resting state (Model II) distance of 2.78 Å to that of the transition-state (Model I) distance of 2.65 Å. Further reduction of the N−O distance changes the energy very little. The energy stabilization appears to be a consequence of the interaction of the positively charged imidazole and the negatively charged aspartate carboxyl. As the histidine side chain becomes protonated during the formation of the tetrahedral species, the energy lowering calculated here may be an important factor in stabilizing the tetrahedral intermediate during catalysis. A recent paper contains a discussion of the theoretical binding energetics of trifluoromethyl ketone inhibitors at the serine proteinase active site.[31] The model used in that study is very similar to Model I.

To calculate the vibrationally averaged chemical shift, the potential for proton transfer from His^{57} $N^{\delta 1}$ to Asp^{102} $O^{\delta 1}$ is required. The full geometry optimization of Model I took 97.7 cpu days on an SGI R10000 computer. Clearly, the use of a

(45) Brady, K.; Liang, T. C.; Abeles, R. H. *Biochemistry* **1989**, *28*, 9066−9070.

(46) Neidhart, D.; Wei, Y.; Cassidy, C.; Lin, J.; Cleland, W. W.; Frey, P. A. *Biochemistry* **2001**, *40*, 2439−2447.

(47) Rhodes, G. *Crystallography made crystal clear*; Academic Press: San Diego, CA, 1993; p 160.

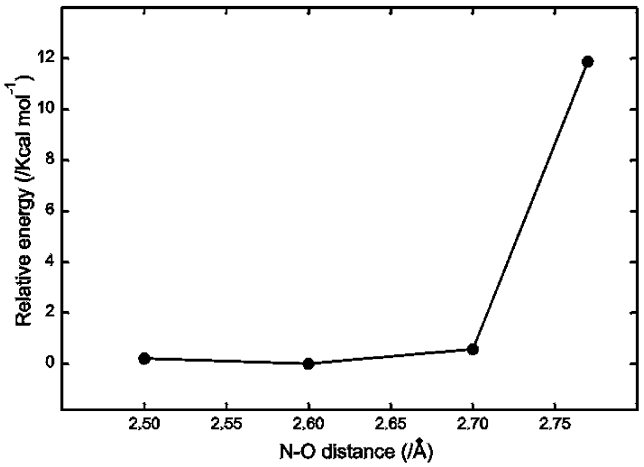

Figure 7. Relative energies (/kcal) for equilibrium proton geometries at various Asp $O^{\delta 1}$–His $N^{\delta 1}$ distances in Model III, the model that represents the tetrahedral intermediate.

Table 3. Comparison of Experimental and Calculated Chemical Shifts for Assigned Resonances of His^{57} in Chymotrypsinogen

atom	experimental chemical shifts (/ppm)[a]	calculated chemical shifts (/ppm)[b]
$H^{\delta 2}$	7.26	6.89
$H^{\epsilon 1}$	9.25	9.02
H	10.60	10.22
$H^{\epsilon 2}$	13.20	12.96
$H^{\delta 1}$	18.20	18.82

[a] Values from ref 11. [b] Model III was modified by replacing the water molecule that represents the side chain hydroxyl of Ser^{214} with β-hydroxybutaraldehyde. The carbonyl of Ser^{214} is proximal to the His^{57} $H^{\epsilon 1}$ atom in crystal structures and this modification of the model gives calculated chemical shift values for $H^{\epsilon 1}$ that are closer to the experimental values than models without the carbonyl moiety.

simpler model that is more computationally friendly is useful to evaluate the effects of vibrational averaging on the chemical shift. Model III (Figure 4B) was chosen as a simpler version of Model I to investigate the tetrahedral intermediate state. This state is not stable to unconstrained geometry optimization, but calculated chemical shifts of the His^{57} protons are close to those found experimentally for protonated chymotrypsinogen (Table 3), and thus one would expect that trends from this model are probably a reasonable description of the physical situation. One disadvantage of using this state is that no proper transition state for proton transfer can be obtained, since geometry optimization of all atoms is required for this. The potential for His^{57} $H^{\delta 1}$ was obtained by placing the proton at intermediate distances between the Asp^{102} $O^{\delta 1}$ and the His^{57} $N^{\delta 1}$ and allowing the orthogonal degrees of freedom to optimize. All other protons bound to either O or N were also unconstrained during the optimization.

The potentials from Model III a–d (Figure 5) show a general trend: as the N–O distance decreases, the probability distribution broadens. Until the N–O distance reaches the smallest value (2.5 Å), the potential remains an asymmetric double-well, and the proton is confined mostly to the well nearest the His^{57} $N^{\delta 1}$. For the tetrahedral intermediate to possess a low-barrier hydrogen bond, the N–O distance would need to be near 2.5 Å. The asymmetric nature of the potential suggests that the pK_a values of Asp^{102} and His^{57} are nonequivalent and, therefore, are not good candidates for a low-barrier hydrogen bond.[33,48] Although the calculated chemical shifts for Model IIIa–d are larger than the experimental value, a definite trend can be discerned. For N–O distances near 2.5 Å, the chemical shifts of His^{57} $H^{\delta 1}$ in Model IIIa–d (Figure 6A) show a weak dependence with respect to distance. By contrast, the dependence of the chemical shift with respect to the N–O distance near 2.7 Å is rather steep (Figure 6B). The opposite behavior is seen for the $^1H-^3H$ isotope shifts, where a steep dependence is seen at short N–O distances, whereas a rather flat dependence is observed for longer distances. Experimentally, higher association constants are correlated with small, but significant, downfield chemical shifts for His^{57} $H^{\delta 1}$ (~0.3 ppm, Table 2). The $^1H-^3H$ isotope shifts are, however, rather insensitive to the identity of the inhibitor. This is similar to the behavior of the chemical shifts and isotope shifts for the structures with an N–O distance near 2.7 Å. The X-ray structures of chymotrypsin in complex with three trifluoromethyl ketone inhibitors show a slight trend for the N–O distance to become shorter with tighter binding inhibitors. Although the distance changes are close to the expected resolution, the downfield chemical shift in the tighter complexes also suggests that the hydrogen-bond distance may shorten with increased association constants.[49] The results of the calculations presented here are consistent with the experimental results provided that the distance between the Asp^{102} $O^{\delta 1}$ and the His^{57} $N^{\delta 1}$ decreases slightly upon binding inhibitors with higher association constants.

In summary, the calculated strength of the Asp^{102} $O^{\delta 1}$ hydrogen bond increases by about 11 kcal mol^{-1} on going from the model of the resting state model to that of the tetrahedral state. This would constitute an important source of transition-state stabilization. Results presented here suggest that the N–O distance in the serine proteinase transition state is about 2.65 Å, somewhat longer than the calculated minimum distance for an LBHB (2.5 Å) for this system.

Acknowledgment. Supported by NIH Grant RR02301 from the Biotechnology Program of the National Center for Research Resources and the College of Agricultural and Life Sciences, University of Wisconsin. W.M.W. would like to thank Professor Ned Seibert for a useful discussion and also pointing out the DVR method for calculation of the eigenstates of the one-dimensional potentials.

JA027735J

(48) Gerlt, J. A.; Kreevoy, M. M.; Cleland, W. W.; Frey, P. A. *Chem. Biol.* **1997**, *4*, 259–267.
(49) Harris, T. K.; Mildvan, A. S. *Proteins: Struct., Funct., Genet.* **1999**, *35*, 275–282.
(50) Lin, J.; Cassidy, C. S.; Frey, P. A. *Biochemistry* **1998**, *37*, 11940–11948.